Published in final edited form as:
Dev Cell. 2011 November 15; 21(5): 966–974. doi:10.1016/j.devcel.2011.08.016.

Autophagy proteins regulate the secretory component of osteoclastic bone resorption

Carl J. DeSelm[1,†], **Brian C. Miller**[1,†], **Wei Zou**[1], **Wandy L. Beatty**[2], **Helena van Meel**[4], **Yoshifumi Takahata**[1], **Judith Klumperman**[4], **Sharon A. Tooze**[5], **Steven L. Teitelbaum**[1,3,*], and **Herbert W. Virgin**[1,2,3,*]

[1]Department of Pathology and Immunology, Washington University Medical School, 660 S. Euclid Avenue, St. Louis, Missouri, 63110, USA [2]Department of Molecular Microbiology, Washington University Medical School, 660 S. Euclid Avenue, St. Louis, Missouri, 63110, USA [3]Department of Medicine, Washington University Medical School, 660 S. Euclid Avenue, St. Louis, Missouri, 63110, USA [4]Department of Cell Biology, University Medical Center Utrecht, Heidelberglaan 100, 3584 CX Utrecht, the Netherlands [5]Secretory Pathways Laboratory; London Research Institute Cancer Research UK; London, UK

Summary

Osteoclasts resorb bone via the ruffled border whose complex folds are generated by secretory lysosome fusion with bone-apposed plasma membrane. Lysosomal fusion with the plasmalemma results in acidification of the resorptive microenvironment and release of CatK to digest the organic matrix of bone. The means by which secretory lysosomes are directed to fuse with the ruffled border are enigmatic. We show that proteins essential for autophagy including Atg5, Atg7, Atg4B and LC3, are important for generating the osteoclast ruffled border, the secretory function of osteoclasts and bone resorption *in vitro* and *in vivo*. Further, Rab7 which is required for osteoclast function, localizes to the ruffled border in an Atg5-dependent manner. Thus, autophagy proteins participate in polarized secretion of lysosomal contents into the extracellular space by directing lysosomes to fuse with the plasma membrane. These findings are in keeping with a putative link between autophagy genes and human skeletal homeostasis.

*Address correspondence to: Steven L. Teitelbaum, Ph: 314-454-8463, Fax: 314-454-5505, teitelbs@wustl.edu; Herbert W. Virgin, Ph: 314-362-9223, Fax: 314-362-4096, virgin@wustl.edu.
†These authors contributed equally
*Co-corresponding authors, contributed equally

Supplemental Information: Supplemental Information includes three figures and additional detailed experimental methods and can be found at doi:_____.

The authors have no financial conflicts of interest.

Author Contributions The original hypothesis was formulated by CJD, BCM, HWV, and SLT. CJD and BCM performed almost all experiments. WZ provided experimental assistance. YT performed *in vitro* bone nodule assays. WLB performed electron microscopy and GFP-LC3 immunoelectron microscopy experiments. EvM and JK performed CatK immunoelectron microscopy experiments. The manuscript was written by CJD, BCM, HWV, and SLT; all authors commented on the manuscript, data, and conclusions before submission.

Introduction

Osteoclasts degrade bone by directionally secreting lysosomal enzymes and HCl into an extracellular resorptive space (Stenbeck, 2002; Zhao et al., 2008a). In this process, secretory lysosomes target an area of bone-apposed plasmalemma confined by an actin ring generating the osteoclast's resorptive organelle, the ruffled border. Fusion of secretory lysosomes to the ruffled border directionally discharges matrix-degrading molecules such as cathepsin K (CatK) into the site of bone degradation. Ruffled border formation requires synaptotagmin VII and Rab7 (Zhao et al., 2001; Zhao et al., 2008a) but other proteins generating this secretory organelle are enigmatic.

Autophagosomes, like the ruffled border, fuse with lysosomes. Autophagosomes are coating with phosphatidylethanolamine (PE)-conjugated LC3-β (termed LC3II herein) (Levine et al., 2011), one of eight mammalian ATG8 family of proteins. This occurs via the action of two ubiquitin-like systems involving Atg5, Atg7, and Atg4B (Weidberg et al., 2010; Levine et al., 2011; Weidberg et al., 2011). Atg7 initiates Atg5-Atg12 conjugation as well as LC3I lipidation to form LC3II. The Atg5-Atg12 conjugate complexes with Atg16L1 to localize production of LC3II which promotes autophagosome elongation, closure, and fusion. The autophagy proteins Atg5, Atg7, and Atg4B/LC3, which regulate fusion of lysosomes with phagosomes (Sanjuan et al., 2007; Huang et al., 2009; Lee et al., 2010), are also important for the function of a range of secretory cells (Cadwell et al., 2008; Ebato et al., 2008; Ganesan et al., 2008; Jung et al., 2008; Marino et al., 2010; Ushio et al., 2011). Furthermore, human genome-wide association data suggests a link between autophagy genes, human height and osteoporosis (Pan et al., 2010; Zhang et al., 2010). Together these considerations led us to hypothesize that autophagy proteins participate in directional release of lysosome-residing resorptive molecules by osteoclasts. Here we report that this is the case.

Results

Lipidated LC3 Localization to the Osteoclast Ruffled Border is Atg5-Dependent

To localize LC3-β (LC3) in osteoclasts, we cultured marrow of GFP-LC3 transgenic mice (Mizushima et al., 2004) on bone fragments in the presence of M-CSF and RANK ligand (RANKL) (Teitelbaum and Ross, 2003). GFP-LC3 concentrated within actin rings in about 30% of cells (e.g. Fig. 1A,B). It also co-localized with CatK at the site of bone degradation (Yamaza et al., 1998), but not outside the confines of the actin ring (Fig. 1A) establishing that secretory lysosomes are not LC3-coated. Immunoelectron microscopy showed LC3 directly associated with the ruffled border (Fig. 1C-D). GFP-LC3+ autophagosomes were apparent in osteoclasts (Fig. S1A), but not in the vicinity of the resorptive organelle. LC3 localization to autophagosomes requires PE conjugation to glycine 120. Failure of the non-conjugatable mutant, GFP-LC3^{G120A} to efficiently localize within actin rings (Fig. 1B), indicates that lipidation mediates delivery of LC3II to the ruffled border.

PE conjugation to LC3I requires Atg5 (Levine et al., 2011). To determine the role of Atg5 in LC3II localization to the ruffled border, we bred *Atg5$^{flox/flox}$* mice to those expressing Cre recombinase under control of the lysozyme M promoter (LyzM-Cre) (Zhao et al., 2008b). Autophagy in *Atg5$^{flox/flox}$*-LyzM-*Cre*+ (Atg5-deficient) osteoclasts was defective as manifest by accumulation of p62 and decreased LC3II (Fig. 1E). Atg5-deletion did not impact osteoclast development, differentiation marker expression, number of nuclei, actin ring formation, ATP levels, or total protein ubiquitination (Fig. S1B-G), and ultrastructural examination revealed no irregularities of mitochondria or intracellular membranes (data not shown). GFP-LC3, however, failed to efficiently localize to the ruffled border in mutant osteoclasts (Fig. 1F-G). Therefore, Atg5 is required for LC3 targeting to the ruffled border.

Atg5 and Atg7 Optimize Bone Resorption

Establishing that autophagy proteins regulate bone degradation, the depth and volume of pits excavated by Atg5-deficient osteoclasts were reduced 2-2.5 fold (Salo et al., 1997) (Fig. 2A-C). Similar to those lacking Atg5, absence of Atg7 inhibited conversion of LC3I to LC3II and dampened resorptive capacity (Fig. 2D-E, S2A). The magnitude of bone pit depth reduction consequent to Atg5 or Atg7 deficiency was similar to that observed with deletion of CatK or the αvβ3 integrin which are required for efficient osteoclast function (Saftig et al., 1998; Mchugh et al., 2000).

Atg5 and Atg7 are Required for Lysosomal Secretion at the Ruffled Border

LAMP1, an integral membrane protein, is delivered to the ruffled border via fusion of secretory lysosomes containing CatK (Palokangas et al., 1997; Maeda et al., 1999). The localization of LAMP1 and CatK within actin rings was reduced approximately 60% in the absence of Atg5 (Fig. 2F-G) or Atg7 (Fig. 2H). Thus, osteoclasts deficient in either gene fail to normally deliver bone-degrading lysosomes to the ruffled border. While these data indicate direct autophagy protein participation in osteoclast function, alternative explanations are possible. Defective secretion by autophagy-deficient vestibular cells is associated with reduced adaptor protein complex 3 (AP-3) (Marino et al., 2010) expression, but Atg5 deficiency did not alter AP-3 abundance in osteoclasts (Fig. S2B). Experiments using fluorescent dextran-3000, which accumulates in the resorptive space where it is endocytosed and then transcytosed to the non-bone apposed surface (Palokangas et al., 1997; Stenbeck and Horton, 2004), revealed no role of Atg5 in endosome uptake and trafficking (Fig. S2C). Atg5 deficiency did not modify synthesis or activation of CatK (Rieman et al., 2001) (Fig. S2D). Secretory lysosome accumulation of CatK was unaltered in Atg5-deficient osteoclasts (Fig. S2E) (Van Meel et al., 2011). We observed secretory lysosomes fusing with the plasma membrane in Atg5-deficient and control osteoclasts cultured on plastic, establishing that Atg5 is not required for lysosome fusion to the plasma membrane in non-polarized cells.

The structure of the ruffled border is deranged in the absence of proteins regulating its formation (Mchugh et al., 2000; Zhao et al., 2008a). Using the actin ring as localization marker, two blinded observers graded ruffled borders in *Atg5*$^{flox/flox}$ and *Atg5*$^{flox/flox}$-LyzM-*Cre+* mice *in vivo*, as absent, immature, or mature (Fig. 3A). Atg5-deficient osteoclasts exhibit a ~20-fold deficiency in mature ruffled border formation (Fig. 3B).

Atg5-Atg12 Conjugation and Atg4B are Necessary for Efficient Lysosome Localization and Bone Resorption

Autophagy requires Atg7-dependent conjugation of Atg5^{K130} to Atg12. To determine if this lysine regulates bone resorption, we expressed wild type Atg5 or Atg5^{K130R} (Mizushima et al., 2001; Hamacher-Brady et al., 2007) in Atg5-deficient osteoclasts. Atg5 but not Atg5^{K130R} was conjugated to Atg12 (Fig. 3C). Only wildtype Atg5 rescued LC3II generation, CatK localization, and bone pit formation by Atg5-deficient cells (Fig. 3C-E). Atg5^{K130R} expression decreased bone pit depth and induced abnormal CatK localization in control osteoclasts, consistent with a dominant-negative effect noted in other cell types (Pyo et al., 2005; Hamacher-Brady et al., 2007). Thus Atg5-12 conjugation is required for osteoclast secretion.

Since LC3 conjugation to PE is not the only function of the Atg5-Atg12 complex (Levine et al., 2011), we expressed a dominant negative mutant of Atg4B (Atg4B^{C74A}), which binds LC3 and blocks its recognition of PE (Fig. S3A), thus inhibiting autophagy without disrupting the Atg5-Atg12 conjugate (Fujita et al., 2008). Atg4B^{C74A} expression reduced bone pit excavation, mislocalized CatK, and inhibited LC3 trafficking to the ruffled border

in control osteoclasts (Fig. 3F-H). LC3 processing is therefore required for efficient osteoclast secretion and bone resorption.

Rab7 generates the ruffled border, modulates bone resorption and promotes autophagosome maturation (Zhao et al., 2001; Harrison et al., 2003; Gutierrez et al., 2004; Jager et al., 2004; Yamaguchi et al., 2009; Tabata et al., 2010). Indicating that ruffled border formation by this small GTPase is Atg5-dependent, Rab7 appeared at the ruffled border in 60% of control osteoclasts, but only 16% of those lacking Atg5 (Fig. 3I, S3B). In comparison, Rab7 localization to the area surrounding the actin ring does not require Atg5 (Fig. S3B).

Requirements for Atg5-dependent osteoclast function in vivo

To assess the physiological significance of Atg5-dependent osteoclast function we measured the bone mass of *Atg5*$^{flox/flox}$ and *Atg5*$^{flox/flox}$-LyzM-*Cre*+ mice. Microcomputerized tomography revealed a small but significant increase in trabecular bone volume in 8 week old *Atg5*$^{flox/flox}$-LyzM-*Cre*+ mice (Fig. 4A) which was more substantial at 8 months (Fig. 4B). As observed in states of impaired osteoclast function such as osteopetrosis, the number of Atg5-deficient osteoclasts was increased in vivo (Fig. 4C-D) (Soriano et al., 1991; Mchugh et al., 2000). Confirming that osteoblast function characteristically parallels that of osteoclasts in vivo (Novack and Teitelbaum, 2008), serum osteocalcin was diminished >50% in mice with Atg5-deficient osteoclasts (Fig. 4E). As expected, Atg5 deletion in myeloid cells did not alter bone formation by osteoblasts in vitro (Fig. 4F). This reduction in osteogenesis in vivo would dampen increases in bone mass expected in face of ineffective Atg5-deficient osteoclasts (Zhao et al., 2008a). Ovariectomy-induced bone loss was reduced about 50% in *Atg5*$^{flox/flox}$-LyzM-*Cre*+ mice due to inhibited resorption (Fig. 4G-H). Thus, Atg5 regulates osteoclast function in physiological and pathological circumstances.

Discussion

The genesis of the ruffled border was enigmatic until it was shown to contain lysosomal proteins (Baron et al., 1988) suggesting that it is the product of fusion of secretory vesicles to the bone-apposed plasma membrane which proved true (Zhao et al., 2008a). Here we address the importance of the autophagy proteins Atg5, Atg7, and Atg4B/LC3 in this process which occurs in conjunction with recruitment of Rab7, which also regulates autophagosome and phagosome maturation and bacterial autophagy, to the ruffled border.

Autophagy and directional secretion of lysosomal contents at the ruffled border require lysosome fusion to a selected membrane. Likewise, autophagy proteins regulate union of phagosomes and lysosomes (Sanjuan et al., 2007; Huang et al., 2009; Lee et al., 2010). In all three processes, a target, cytoplasm-exposed membrane is marked by PE-conjugated LC3 generated by systems involving Atg5, Atg7, and Atg4B. Therefore, these autophagy proteins may, by directing LC3 to specific sites, prevent indiscriminate fusion of lysosomes to intracellular membranes.

Autophagy protein-deficient osteoclasts resorb bone poorly, exhibit impaired localization of CatK and LAMP1 within the actin ring, and lack normal ruffled borders, likely reflecting failed secretory lysosome/plasma membrane fusion. While Atg5 regulates ruffled border development it does not impact generation of the secretory lysosomes from which it is derived. We considered the possibility that the osteoclast ruffled border is a product of classical autophagy, or that deficient lysosomal secretion observed here reflected abnormal homeostasis in Atg5-deficient cells. However, Atg5 deficiency did not alter osteoclast differentiation, secretory lysosome biogenesis, formation of actin rings, organelle or morphology, ATP content or total ubiquitination.

Inhibited localization of LC3 to the ruffled border, by deleting Atg5 or over-expressing dominant negative Atg4B, correlates with dampened bone resorption. LC3-$\beta^{-/-}$ osteoclasts, however, effectively concentrate CatK within actin rings and have normal bone mass (data not shown), perhaps reflecting compensation by other ATG8 family members. LC3 could be delivered to the ruffled border by fusion with organelles expressing this autophagy protein, but LC3 and lysosome-residing CatK do not co-localize outside of the resorptive microenvironment indicating that secretory lysosomes are not LC3-coated. We observed no autophagosomes in the vicinity of the ruffled border nor extracellular cytoplasmic debris, potentially released by autophagosome fusion to the ruffled border, in the resorptive microenvironment. Perhaps the most compelling evidence suggesting that autophagosomes do not directly contribute to the ruffled border is the fact that CatK and LAMP1, which are secretory lysosome- and not autophagosome-associated molecules, are delivered to this membrane in an autophagy protein-dependent process.

p62 modulates NF-κB, an important osteoclastogenic transcription factor and p62 mutations are associated with Paget's disease of bone, a disorder of overzealous osteoclasts (Kurihara et al., 2011). Atg5-deficient osteoclasts accumulate p62, but our findings suggest the cell's phenotypic abnormalities do not reflect this excess. In contrast to those lacking Atg5, for example, nuclear number decreases in p62 over-expressing osteoclasts which are also unable to effectively form actin rings (Yip et al., 2006; Chamoux et al., 2009).

Our findings add to emerging evidence that autophagy proteins participate in cell secretion and suggest a mechanism by which this occurs. Autophagy proteins participate in a non-classical secretory process in *Pichia pastoris* and *Dictyostelium discoideum* (Duran et al., 2010; Manjithaya et al, 2010), potentially via union of autophagosomes and the plasma membrane. This event differs from fusion of single membrane-bound secretory lysosomes to the plasmalemma studied here. Autophagy protein deficiency also impairs secretion of lysozyme from Paneth cells (Cadwell et al., 2008; Cadwell et al., 2010), insulin from pancreatic β-cells (Ebato et al., 2008; Jung et al., 2008), melanosomes (which are considered lysosome-related organelles) from melanocytes (Ganesan et al., 2008), mast cell mediators (Ushio et al., 2011), and otoconial proteins from vestibular epithelial cells (Marino et al., 2010). While these data support a general role for certain autophagy proteins in secretion, the mechanisms responsible may be cell type-specific.

Pathway analysis based on human genome wide association data link autophagy genes to human skeletal homeostasis (Pan et al., 2010; Zhang et al., 2010). Together with our finding that Atg5-deletion protects against experimental post-menopausal osteoporosis, this indicates that autophagy proteins are candidate therapeutic targets for pathological bone loss. Importantly, clinical targeting of these proteins for other purposes may impact the skeleton, suggesting that trial of autophagy-active drugs should evaluate bone health.

Experimental Procedures

Mice and osteoclasts

$Atg5^{flox/flox}$, $Atg7^{flox/flox}$, $Atg5^{flox/flox}$-LyzM-Cre+, LC3-$\beta^{-/-}$, and GFP-LC3 mice have been described (Mizushima et al., 2004; Komatsu et al., 2005; Hara et al., 2006; Cann et al., 2008; Zhao et al., 2008b). Bone marrow macrophages were differentiated into osteoclasts on either plastic or bovine bone slices by culture with M-CSF and RANK ligand as described (Teitelbaum and Ross, 2003; Zhao et al., 2008a). In some experiments bone marrow macrophages were retrovirus transduced using pMXs-IRES-Puro retroviral vector expressing the desired gene (Cell Biolabs, Inc., San Diego, CA), antibiotic selected, and then differentiated into osteoclasts (Zhao et al., 2008a). mCherry-Atg5, mCherry-$Atg5^{K130R}$ (Hamacher-Brady et al., 2007) and mStrawberry-$Atg4B^{C74A}$ (Fujita et al., 2008) constructs

cloned into the retroviral vector were as described. Western blot, electron microscopy, and histology of bones fixed in 4% PFA were as described (Zhao et al., 2008a). Specificity of immunoelectron microscopy was confirmed by staining control osteoclasts with anti-GFP antibody or of GFP-LC3 transgenic cells with an isotype control antibody. FITC-dextran-3000 experiments were as described (Stenbeck and Horton, 2004).

Immunofluorescence

Osteoclasts grown on bone slices were imaged by confocal microscopy (Zhao et al., 2008a) after fixation in 4% paraformaldehyde for 10 minutes and washing with PBS. Cells were permeabilized in 0.1% Triton-X for 10 minutes at room temperature and blocked for 1 hour in PBS containing 0.2% BSA, 10% normal rabbit serum, and 10% normal goat serum (goat serum was replaced with donkey serum if primary antibody was a goat antibody). All antibodies (see Supplement) were diluted in blocking buffer. Primary antibodies were applied overnight. After washing in PBS, secondary antibodies were applied for 1 hour at room temperature. Bones were then mounted in 30% glycerol or VECTASHIELD Mounting Media with DAPI (Vector labs, Burlingame, CA) and imaged on a Nikon Eclipse epifluorescent microscope (Nikon, Melville, NY), Olympus BX51 epifluorescent microscope (Olympus, Center Valley, PA), or Axiovert 100M confocal microscope (Zeiss, Thornwood, NY). Confocal images were analyzed using LSM 510 software (Zeiss, Thornwood, NY). For localization of GFP-LC3, cathepsin K, and LAMP1, confocal microscopy was used to identify cells with complete actin rings. If the area outlined by the actin ring was completely occupied by CatK in any z-plane containing the actin ring, and CatK was not visualized outside the ring in those z-planes, the cell was said to have positive CatK localization. The same procedure was followed for LAMP1, GFP-LC3, and Rab7 localization. All data was collected by a blinded observer.

Nuclei Counts

Osteoclasts were grown on bone for 6 days, fixed and permeabilized as described above. Cells were stained with Alexa 555-conjugated phalloidin and mounted with VECTASHIELD Mounting Media with DAPI to visualize actin rings and nuclei. Nuclei per cell were quantified counting any cell with at least three nuclei.

Actin ring formation

Osteoclasts grown on bone slices were incubated in cold alpha10 media for 30 minutes to disrupt actin rings, followed by warm alpha10 with 10% FBS, RANKL, and M-CSF. Cells were fixed at the indicated times, and actin rings were phalloidin stained and counted.

Bone pit depth measurements

Osteoclast-generated bone pits were stained by removing the cells from thin bone slices with a soft brush and incubating with 20ug/mL FITC conjugated wheat germ agglutinin (Sigma, St. Louis, MO) for 30 minutes at room temperature. After washing the bones, pits were imaged by confocal microscopy. The pit depth was measured from the surface of the bone down to the deepest point in the pit. All data was collected by a blinded observer.

Microcomputed tomography and ovariectomy

Microcomputed tomography (vivaCT 40, Scanco Medical, Brüttisellen, Switzerland) was as described (Zhao et al., 2008a). Trabecular volume in the distal femoral metaphysis (right leg) was measured while mice were anesthetized with isofluorane. A threshold linear attenuation coefficient of 1.2 cm^{-1} was used to differentiate bone from non-bone. A threshold of 120 was used for evaluation of all scans. 30 slices were analyzed, starting with the first slice in which condyles and primary spongiosa were no longer visible. Trabecular

volume was measured one day before ovariectomy or sham operation (basal bone volume) and 28 days after surgery (post-ovx). For ovariectomies, mice were anesthetized with ketamine/xylene delivered by intraperitoneal injection, and ovaries were removed through two small dorsal incisions. Sham operated mice were anesthetized and opened equivalently, but ovaries were not removed.

Osteoblast bone formation assay

Osteoblasts were harvested from the calvariae of 3-day-old *Atg5*$^{flox/flox}$ or *Atg5*$^{flox/flox}$-LyzM-*Cre+* mice by collagenase digestion and cultured for 21 days with differentiation media containing 50 μg/ml ascorbic acid and 2 mM β-glycerophosphate. Bone nodules were stained with Alizarin Red.

Statistics

All data was analyzed with Prism software (Graphpad, San Diego, CA), using two-tailed unpaired Student's t tests, unless otherwise indicated. Error bars represent standard deviation.

Supplementary Material

Refer to Web version on PubMed Central for supplementary material.

Acknowledgments

HWV was supported by U54 AI057160 Project 5 and RO1 AI0848887; SLT was supported by AR057235, AR032788, AR057037, AR046523, and AR054618; CJD was supported by AG032795, from National Institutes of Health, and the contents of this study are solely the responsibility of the authors and do not necessarily represent the official views of the NIH. EvM and JK were supported by VICI grant 918.56.611 of the Netherlands Organization for Scientific Research (NWO). We thank Karen Green for assistance with electron microscopy, and René Scriwanek, Viola Oorschot, and Marc van Peski for preparation of the CatK immunoelectron micrographs.

References

Baron R, Neff L, Brown W, Courtoy PJ, Louvard D, Farquhar M. Polarized secretion of lysosomal enzymes: Co-distribution of cation-independent mannose-6-phosphate receptors and lysosomal enzymes along the osteoclast exocytic pathway. J Cell Biol. 1988; 106:1863–1872. [PubMed: 2968345]

Cadwell K, Liu JY, Brown SL, Miyoshi H, Loh J, Lennerz JK, Kishi C, Kc W, Carrero JA, Hunt S, et al. A key role for autophagy and the autophagy gene Atg16l1 in mouse and human intestinal Paneth cells. Nature. 2008; 456:259–263. [PubMed: 18849966]

Cadwell K, Patel KK, Maloney NS, Liu TC, Ng AC, Storer CE, Head RD, Xavier R, Stappenbeck TS, Virgin HW. Virus-plus-susceptibility gene interaction determines Crohn's disease gene Atg16L1 phenotypes in intestine. Cell. 2010; 141:1135–1145. [PubMed: 20602997]

Cann GM, Guignabert C, Ying L, Deshpande N, Bekker JM, Wang L, Zhou B, Rabinovitch M. Developmental expression of LC3alpha and beta: absence of fibronectin or autophagy phenotype in LC3beta knockout mice. Dev Dyn. 2008; 237:187–195. [PubMed: 18069693]

Chamoux E, Couture J, Bisson M, Morissette J, Brown JP, Roux S. The p62 P392L mutation linked to Paget's disease induces activation of human osteoclasts. Mol Endocrinol. 2009; 23:1668–1680. [PubMed: 19589897]

Duran JM, Anjard C, Stefan C, Loomis WF, Malhotra V. Unconventional secretion of Acb1 is mediated by autophagosomes. J Cell Biol. 2010; 188:527–536. [PubMed: 20156967]

Ebato C, Uchida T, Arakawa M, Komatsu M, Ueno T, Komiya K, Azuma K, Hirose T, Tanaka K, Kominami E, et al. Autophagy is important in islet homeostasis and compensatory increase of beta cell mass in response to high-fat diet. Cell Metab. 2008; 8:325–332. [PubMed: 18840363]

Fujita N, Hayashi-Nishino M, Fukumoto H, Omori H, Yamamoto A, Noda T, Yoshimori T. An Atg4B mutant hampers the lipidation of LC3 paralogues and causes defects in autophagosome closure. Mol Biol Cell. 2008; 19:4651–4659. [PubMed: 18768752]

Ganesan AK, Ho H, Bodemann B, Petersen S, Aruri J, Koshy S, Richardson Z, Le LQ, Krasieva T, Roth MG, et al. Genome-wide siRNA-based functional genomics of pigmentation identifies novel genes and pathways that impact melanogenesis in human cells. PLoS Genet. 2008; 4:e1000298. [PubMed: 19057677]

Gutierrez MG, Munafo DB, Beron W, Colombo MI. Rab7 is required for the normal progression of the autophagic pathway in mammalian cells. J Cell Sci. 2004; 117:2687–2697. [PubMed: 15138286]

Hamacher-Brady A, Brady NR, Logue SE, Sayen MR, Jinno M, Kirshenbaum LA, Gottlieb RA, Gustafsson AB. Response to myocardial ischemia/reperfusion injury involves Bnip3 and autophagy. Cell Death Differ. 2007; 14:146–157. [PubMed: 16645637]

Hara T, Nakamura K, Matsui M, Yamamoto A, Nakahara Y, Suzuki-Migishima R, Yokoyama M, Mishima K, Saito I, Okano H, et al. Suppression of basal autophagy in neural cells causes neurodegenerative disease in mice. Nature. 2006; 441:885–889. [PubMed: 16625204]

Harrison RE, Bucci C, Vieira OV, Schroer TA, Grinstein S. Phagosomes fuse with late endosomes and/or lysosomes by extension of membrane protrusions along microtubules: role of Rab7 and RILP. Mol Cell Biol. 2003; 23:6494–6506. [PubMed: 12944476]

Huang J, Canadien V, Lam GY, Steinberg BE, Dinauer MC, Magalhaes MA, Glogauer M, Grinstein S, Brumell JH. Activation of antibacterial autophagy by NADPH oxidases. Proc Natl Acad Sci U S A. 2009; 106:6226–6231. [PubMed: 19339495]

Jager S, Bucci C, Tanida I, Ueno T, Kominami E, Saftig P, Eskelinen EL. Role for Rab7 in maturation of late autophagic vacuoles. J Cell Sci. 2004; 117:4837–4848. [PubMed: 15340014]

Jung HS, Chung KW, Won Kim J, Kim J, Komatsu M, Tanaka K, Nguyen YH, Kang TM, Yoon KH, Kim JW, et al. Loss of autophagy diminishes pancreatic beta cell mass and function with resultant hyperglycemia. Cell Metab. 2008; 8:318–324. [PubMed: 18840362]

Komatsu M, Waguri S, Ueno T, Iwata J, Murata S, Tanida I, Ezaki J, Mizushima N, Ohsumi Y, Uchiyama Y, et al. Impairment of starvation-induced and constitutive autophagy in Atg7-deficient mice. J Cell Biol. 2005; 169:425–434. [PubMed: 15866887]

Kurihara N, Hiruma Y, Yamana K, Michou L, Rousseau C, Morissette J, Galson DL, Teramachi J, Zhou H, Dempster DW, et al. Contributions of the measles virus nucleocapsid gene and the SQSTM1/p62(P392L) mutation to Paget's disease. Cell Metab. 2011; 13:23–34. [PubMed: 21195346]

Lee HK, Mattei LM, Steinberg BE, Alberts P, Lee YH, Chervonsky A, Mizushima N, Grinstein S, Iwasaki A. In vivo requirement for Atg5 in antigen presentation by dendritic cells. Immunity. 2010; 32:227–239. [PubMed: 20171125]

Levine B, Mizushima N, Virgin HW. Autophagy in immunity and inflammation. Nature. 2011; 469:323–335. [PubMed: 21248839]

Maeda H, Akasaki K, Yoshimine Y, Akamine A, Yamamoto K. Limited and selective localization of the lysosomal membrane glycoproteins LGP85 and LGP96 in rat osteoclasts. Histochem Cell Biol. 1999; 111:245–251. [PubMed: 10219623]

Manjithaya R, Anjard C, Loomis WF, Subramani S. Unconventional secretion of Pichia pastoris Acb1 is dependent on GRASP protein, peroxisomal functions, and autophagosome formation. J Cell Biol. 2010; 188:537–546. [PubMed: 20156962]

Marino G, Fernandez AF, Cabrera S, Lundberg YW, Cabanillas R, Rodriguez F, Salvador-Montoliu N, Vega JA, Germana A, Fueyo A, et al. Autophagy is essential for mouse sense of balance. J Clin Invest. 2010; 120:2331–2344. [PubMed: 20577052]

Mchugh KP, Hodivala-Dilke K, Zheng MH, Namba N, Lam J, Novack D, Feng X, Ross FP, Hynes RO, Teitelbaum SL. Mice lacking β3 integrins are osteosclerotic because of dysfunctional osteoclasts. J Clin Invest. 2000; 105:433–440. [PubMed: 10683372]

Mizushima N, Yamamoto A, Hatano M, Kobayashi Y, Kabeya Y, Suzuki K, Tokuhisa T, Ohsumi Y, Yoshimori T. Dissection of autophagosome formation using Apg5-deficient mouse embryonic stem cells. J Cell Biol. 2001; 152:657–668. [PubMed: 11266458]

Mizushima N, Yamamoto A, Matsui M, Yoshimori T, Ohsumi Y. In vivo analysis of autophagy in response to nutrient starvation using transgenic mice expressing a fluorescent autophagosome marker. Mol Biol Cell. 2004; 15:1101–1111. [PubMed: 14699058]

Novack DV, Teitelbaum SL. The osteoclast: friend or foe? Annu Rev Pathol. 2008; 3:457–484. [PubMed: 18039135]

Palokangas H, Mulari M, Vaananen HK. Endocytic pathway from the basal plasma membrane to the ruffled border membrane in bone-resorbing osteoclasts. J Cell Sci. 1997; 110:1767–1780. [PubMed: 9264464]

Pan F, Liu XG, Guo YF, Chen Y, Dong SS, Qiu C, Zhang ZX, Zhou Q, Yang TL, Guo Y, et al. The regulation-of-autophagy pathway may influence Chinese stature variation: evidence from elder adults. J Hum Genet. 2010; 55:441–447. [PubMed: 20448653]

Pyo JO, Jang MH, Kwon YK, Lee HJ, Jun JI, Woo HN, Cho DH, Choi B, Lee H, Kim JH, et al. Essential roles of Atg5 and FADD in autophagic cell death: dissection of autophagic cell death into vacuole formation and cell death. J Biol Chem. 2005; 280:20722–20729. [PubMed: 15778222]

Rieman DJ, Mcclung HA, Dodds RA, Hwang SM, Holmes MW, James IE, Drake FH, Gowen M. Biosynthesis and processing of cathepsin K in cultured human osteoclasts. Bone. 2001; 28:282–289. [PubMed: 11248658]

Saftig P, Hunziker E, Wehmeyer O, Jones S, Boyde A, Rommerskirch W, Moritz JD, Schu P, Von Figura K. Impaired osteoclastic bone resorption leads to osteopetrosis in cathepsin-K-deficient mice. Proc Natl Acad Sci USA. 1998; 95:13453–13458. [PubMed: 9811821]

Salo J, Lehenkari P, Mulari M, Metsikko K, Vaananen HK. Removal of osteoclast bone resorption products by transcytosis. Science. 1997; 276:270–273. [PubMed: 9092479]

Sanjuan MA, Dillon CP, Tait SW, Moshiach S, Dorsey F, Connell S, Komatsu M, Tanaka K, Cleveland JL, Withoff S, et al. Toll-like receptor signalling in macrophages links the autophagy pathway to phagocytosis. Nature. 2007; 450:1253–1257. [PubMed: 18097414]

Soriano P, Montgomery C, Geske R, Bradley A. Targeted disruption of the c-src proto-oncogene leads to osteopetrosis in mice. Cell. 1991; 64:693–702. [PubMed: 1997203]

Stenbeck G. Formation and function of the ruffled border in osteoclasts. Semin Cell Dev Biol. 2002; 13:285–292. [PubMed: 12243728]

Stenbeck G, Horton MA. Endocytic trafficking in actively resorbing osteoclasts. J Cell Sci. 2004; 117:827–836. [PubMed: 14762112]

Tabata K, Matsunaga K, Sakane A, Sasaki T, Noda T, Yoshimori T. Rubicon and PLEKHM1 negatively regulate the endocytic/autophagic pathway via a novel Rab7-binding domain. Mol Biol Cell. 2010; 21:4162–4172. [PubMed: 20943950]

Teitelbaum SL, Ross FP. Genetic regulation of osteoclast development and function. Nat Rev Genet. 2003; 4:638–649. [PubMed: 12897775]

Ushio H, Ueno T, Kojima Y, Komatsu M, Tanaka S, Yamamoto A, Ichimura Y, Ezaki J, Nishida K, Komazawa-Sakon S, et al. Crucial role for autophagy in degranulation of mast cells. J Allergy Clin Immunol. 2011; 127:1267–1276. e1266. [PubMed: 21333342]

Van Meel E, Boonen M, Zhao H, Oorschot V, Ross FP, Kornfeld S, Klumperman J. Disruption of the man-6-p targeting pathway in mice impairs osteoclast secretory lysosome biogenesis. Traffic (Copenhagen, Denmark). 2011; 12:912–924.

Weidberg H, Shpilka T, Shvets E, Abada A, Shimron F, Elazar Z. LC3 and GATE-16 N Termini Mediate Membrane Fusion Processes Required for Autophagosome Biogenesis. Dev Cell. 2011; 20:444–454. [PubMed: 21497758]

Weidberg H, Shvets E, Shpilka T, Shimron F, Shinder V, Elazar Z. LC3 and GATE-16/GABARAP subfamilies are both essential yet act differently in autophagosome biogenesis. EMBO J. 2010; 29:1792–1802. [PubMed: 20418806]

Yamaguchi H, Nakagawa I, Yamamoto A, Amano A, Noda T, Yoshimori T. An initial step of GAS-containing autophagosome-like vacuoles formation requires Rab7. PLoS Pathog. 2009; 5:e1000670. [PubMed: 19956673]

Yamaza T, Goto T, Kamiya T, Kobayashi Y, Sakai H, Tanaka T. Study of immunoelectron microscopic localization of cathepsin K in osteoclasts and other bone cells in the mouse femur. Bone. 1998; 23:499–509. [PubMed: 9855458]

Yip KH, Feng H, Pavlos NJ, Zheng MH, Xu J. p62 ubiquitin binding-associated domain mediated the receptor activator of nuclear factor-kappaB ligand-induced osteoclast formation: a new insight into the pathogenesis of Paget's disease of bone. Am J Pathol. 2006; 169:503–514. [PubMed: 16877352]

Zhang L, Guo YF, Liu YZ, Liu YJ, Xiong DH, Liu XG, Wang L, Yang TL, Lei SF, Guo Y, et al. Pathway-based genome-wide association analysis identified the importance of regulation-of-autophagy pathway for ultradistal radius BMD. J Bone Miner Res. 2010; 25:1572–1580. [PubMed: 20200951]

Zhao H, Ito Y, Chappel J, Andrews NW, Teitelbaum SL, Ross FP. Synaptotagmin VII regulates bone remodeling by modulating osteoclast and osteoblast secretion. Dev Cell. 2008a; 14:914–925. [PubMed: 18539119]

Zhao H, Laitala-Leinonen T, Parikka V, Vaananen HK. Downregulation of small GTPase Rab7 impairs osteoclast polarization and bone resorption. J Biol Chem. 2001; 276:39295–39302. [PubMed: 11514537]

Zhao Z, Fux B, Goodwin M, Dunay IR, Strong D, Miller BC, Cadwell K, Delgado MA, Ponpuak M, Green KG, et al. Autophagosome-independent essential function for the autophagy protein Atg5 in cellular immunity to intracellular pathogens. Cell Host Microbe. 2008b; 4:458–469. [PubMed: 18996346]

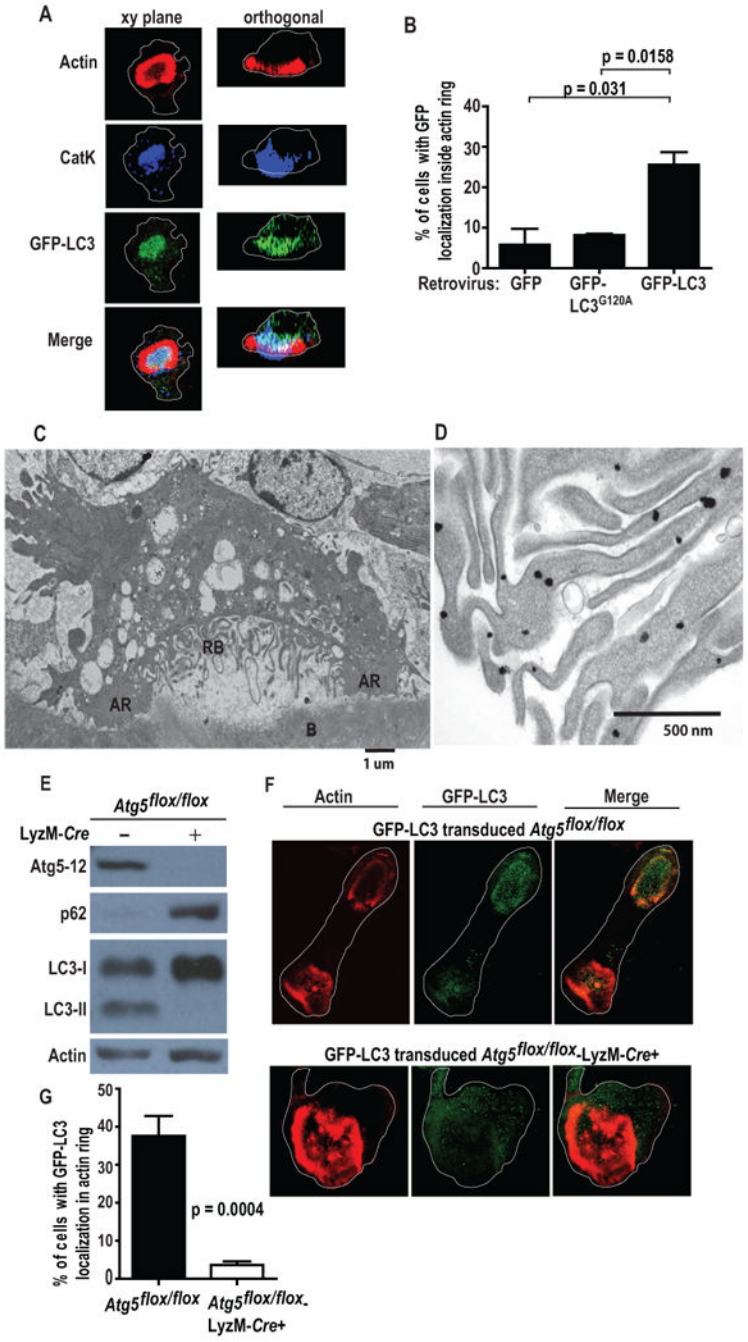

Figure 1. GFP-LC3 localization to the ruffled border is Atg5-dependent

(A) Confocal image of GFP-LC3 transgenic bone-residing osteoclast; CatK, blue; actin, red; GFP, green; cell perimeters, white. CatK and GFP-LC3 localize within the actin ring in the xy and orthogonal planes, representative of two experiments.

(B) Percent of osteoclasts with GFP within the actin ring. Osteoclast precursors were transduced with GFP, GFP-LC3 or GFP-LC3^{G120A} and differentiated on bone for 6 days; n=40, pooled from two experiments.

(C) Electron microscopy of a resorbing osteoclast on bone (B) with a developed ruffled border (RB) surrounded by actin rings (AR).

(D) Immuno-gold labeling of GFP-LC3 in the ruffled border of a resorbing osteoclast.

(E) Western blot of Atg5, p62, LC3, and β-actin in control and Atg5-deficient osteoclasts, representative of 6 experiments.
(F) Bone-residing control and Atg5-deficient osteoclasts transduced with GFP-LC3 visualized by confocal microscopy; actin, green; CatK, red; cell perimeter, white.
(G) Percentage of control and Atg5-deficient osteoclasts with GFP-LC3 concentrated within the actin ring; n=40, pooled from two experiments.

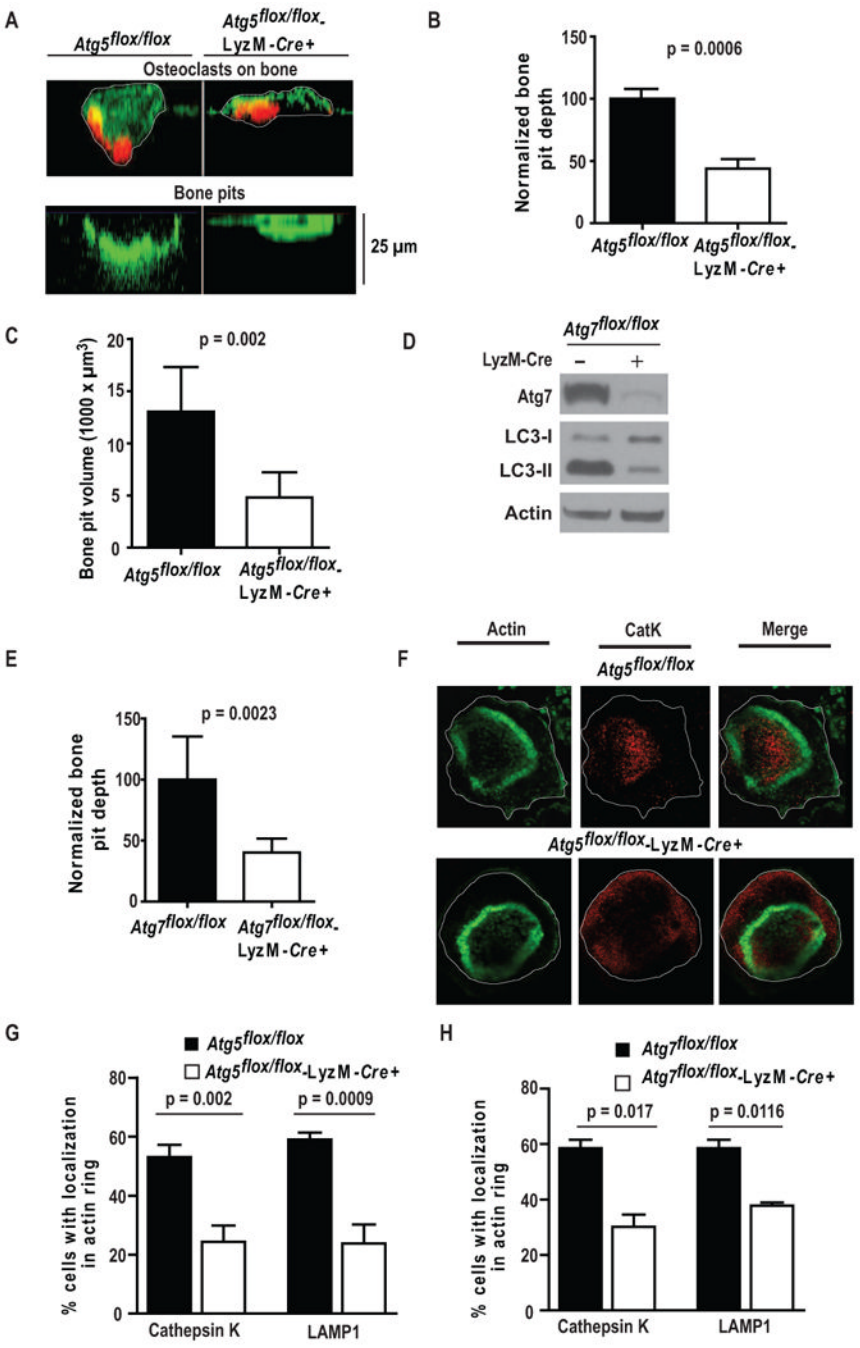

Figure 2. *Atg5*- and *Atg7*-deficient osteoclasts exhibit defective bone pit excavation and lysosome localization to the resorptive microenvironment

(A) Control and Atg5-deficient bone-residing osteoclasts immunostained for actin (red) and exposed to FITC-wheat germ agglutinin (WGA) which stains cells and bone pits green; white, cell perimeters. Bone was visualized in z plane by confocal microscopy before (top) and following removal of cells (bottom), representative of two experiments.

(B) Normalized bone pit depth excavated by control and Atg5-deficient osteoclasts. Data from of four experiments (n=100) was normalized to the average depth excavated by control cells as 100% and analyzed using paired t-test.

(C) 3D confocal images of FITC-WGA-stained bone pits excavated by control and Atg5-deficient osteoclasts used to determine pit volume; LSM software, one of two experiments shown, n=7 per genotype per experiment.
(D) Expression of Atg7, LC3, and β-actin in lysates of control or Atg7-deficient osteoclasts generated for 6 days on plastic; representative of three experiments.
(E) Normalized bone pit depth excavated by control and Atg7-deficient osteoclasts; one of two experiments shown, n=7 per genotype per experiment.
(F) Representative confocal images of control and Atg5-deficient bone-residing osteoclasts; actin, green; CatK, red; cell perimeters, white.
(G) Percentage of control or Atg5-deficient bone-residing osteoclasts with CatK or LAMP1 concentrated within the actin ring; n=45, pooled from three experiments.
(H) Percentage of control or Atg7-deficient bone-residing osteoclasts with CatK or LAMP1 localized in the actin ring; n=30, pooled from two experiments.

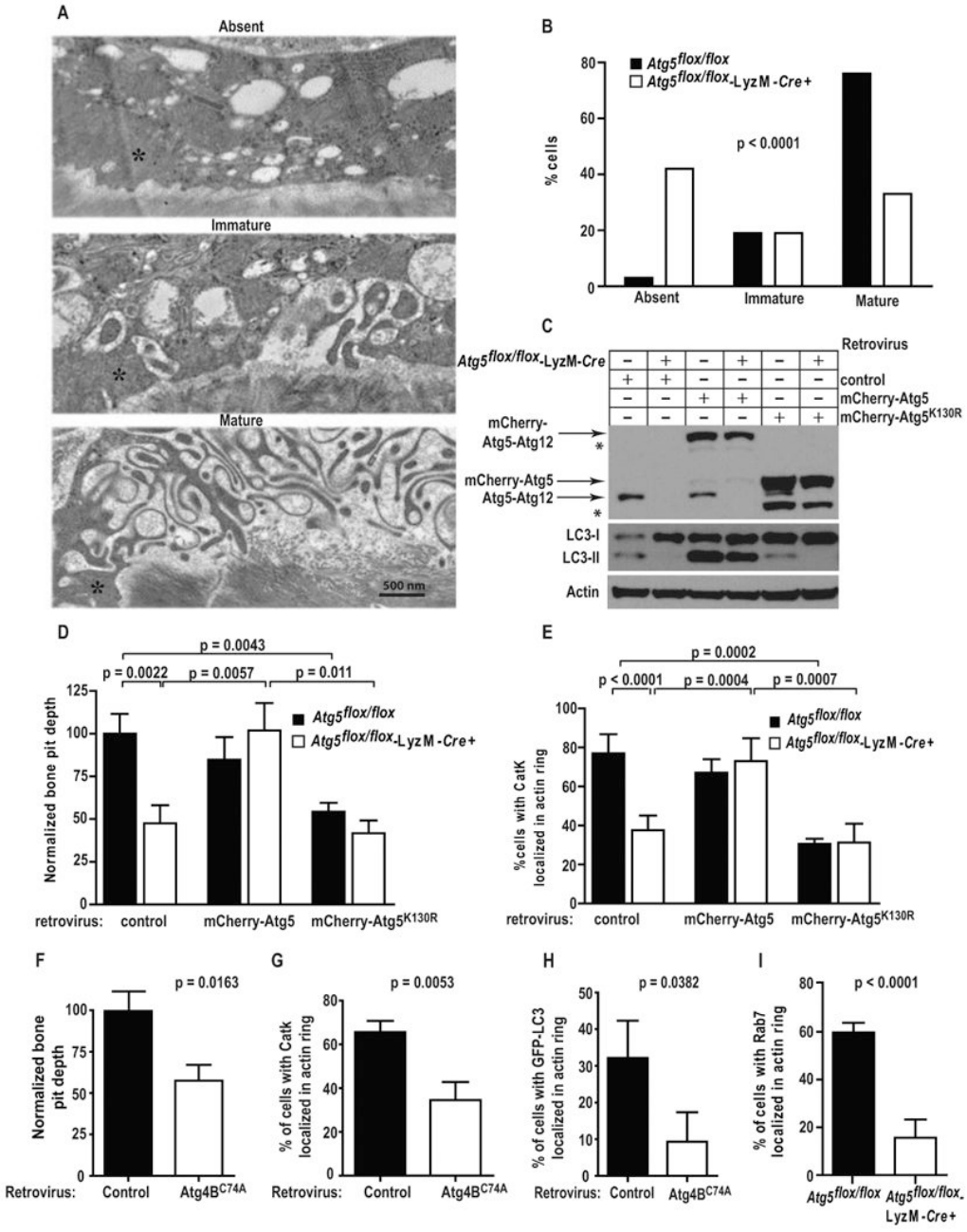

Figure 3. Autophagy proteins mediate ruffled border formation and osteoclast secretory function

(A) Representative electron micrographs of tibia-residing osteoclasts with absent (top), immature (middle), and mature (bottom) ruffled borders adjacent to actin rings (asterisk).

(B) Percentage of control or Atg5-deficient osteoclasts exhibiting absent, immature, or mature ruffled borders; representative of two experiments, analyzed by chi-square test for trend, n=30 cells per mouse per genotype.

(C) Western blots for Atg5, LC3, or β-actin in control or Atg5-deficient osteoclasts transduced with mCherry-Atg5 or mCherry-Atg5^{K130R} encoding retrovirueses; *, unknown bands, representative of three experiments.

(D) Normalized bone pit depth excavated by retrovirally-transduced control or Atg5-deficient osteoclasts; n=20, pooled from three experiments, analyzed by paired t-test.

(E) Percentage of osteoclasts with CatK concentrated within the actin ring in retrovirally-transduced control or Atg5-deficient osteoclasts; n=45, pooled from three experiments.
(F) Normalized bone pit depth excavated by wildtype osteoclasts retrovirally-transduced with empty vector (control) or mStraberry-Atg4BC74A, expressed as a percentage relative to control; n=30, pooled from three experiments, analyzed by paired t-test.
(G) Percentage of cells with CatK localization in actin rings of wildtype osteoclasts transduced with empty vector (control) or $Atg4B^{C74A}$; n=45, representative of three experiments shown.
(H) Percentage of cells with GFP-LC3 localized in the actin ring of vector (control) or $Atg4B^{C74A}$ transduced GFP-LC3 osteoclasts; n=45, representative of two experiments.
(I) Percentage of cells with Rab7 localized in the actin ring of control or Atg5-deficient osteoclasts; n=60, pooled from four experiments.

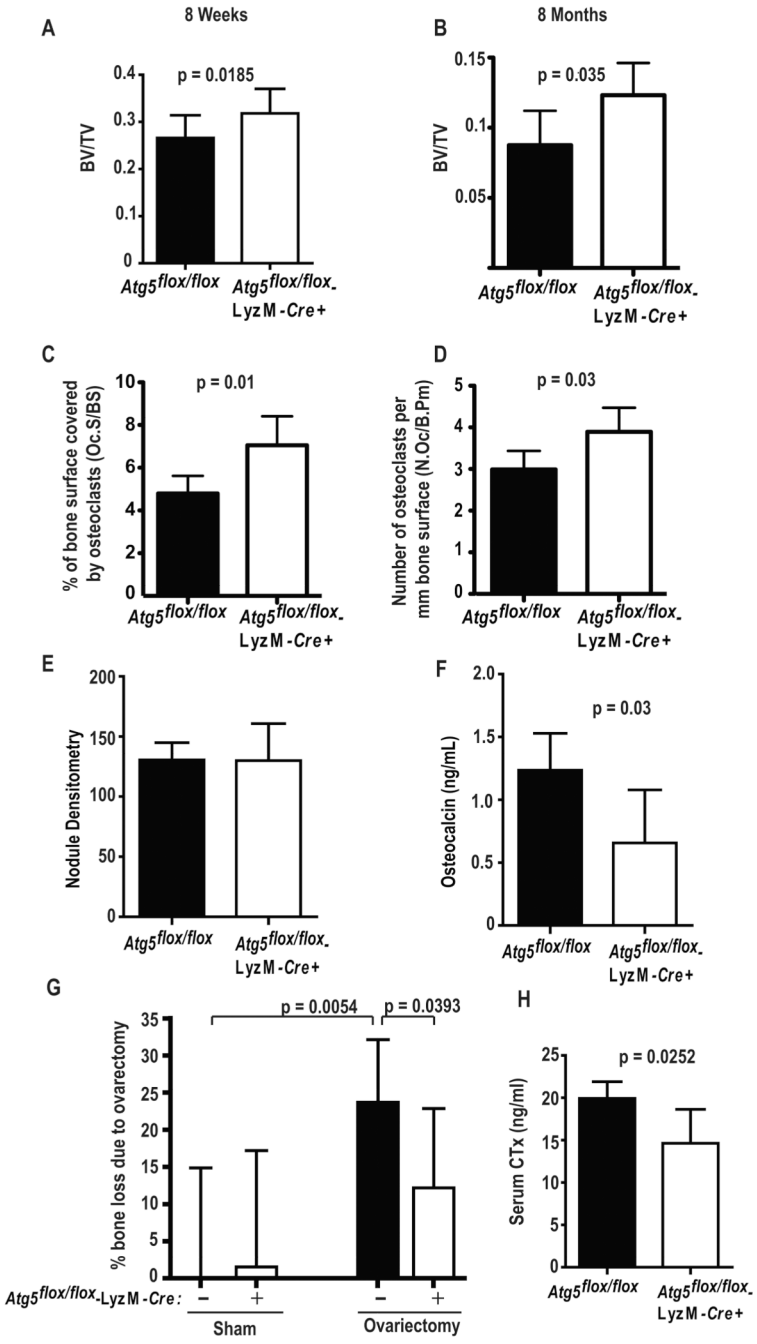

Figure 4. Requirements for Atg5-dependent osteoclast function in vivo

(A, B) Percentage of marrow space occupied by trabecular bone (BV/TV) of 8-week and 8-month old female *Atg5*$^{flox/flox}$ or *Atg5*$^{flox/flox}$-LyzM-*Cre*+ mice by microcomputed tomography; n=12 eight week old mice/genotype, n=6 eight-month old *Atg5*$^{flox/flox}$ mice, n=5 eight month old *Atg5*$^{flox/flox}$-LyzM-*Cre*+ mice.

(C) Percentage of trabecular bone surface covered by TRAP+ osteoclasts determined by histomorphometry; n=5 mice/genotype.

(D) Number of osteoclasts per mm of femoral trabecular bone surface determined by histomorphometry; n=5 mice/genotype.

(E) Serum osteocalcin levels in 8-week old *Atg5*$^{flox/flox}$ (n= 5) and *Atg5*$^{flox/flox}$-LyzM-*Cre*+ mice (n=6) mice.
(F) Bone nodule formation by osteoblasts *in vitro*. Nodules were stained with Alizarin Red-S and quantified using densitometry; pooled from three experiments, n=7 *Atg5*$^{flox/flox}$ mice, n=10 *Atg5*$^{flox/flox}$-LyzM-*Cre*+ mice.
(G) Percentage of bone loss determined by BV/TV in the four weeks following ovariectomy. Ovariectomy (ovx) or sham operation was performed on *Atg5*$^{flox/flox}$ (8 ovx, 5 sham) or *Atg5*$^{flox/flox}$-LyzM-*Cre*+ (7 ovx, 4 sham) mice. The average bone loss of sham-operated *Atg5*$^{flox/flox}$ animals was subtracted from all measurements.
(H) Serum concentration of c-telopeptide of type I collagen (CTx) determined two weeks post-ovariectomy; n=6 mice per genotype.